ACSNANO

www.acsnano.org

ARTICLE

Integrated Three-Dimensional Carbon Paper/Carbon Tubes/Cobalt-Sulfide Sheets as an Efficient Electrode for Overall Water Splitting

Jun Wang,[†,‡] Hai-xia Zhong,[†,‡] Zhong-li Wang,[†] Fan-lu Meng,[†] and Xin-bo Zhang*[,†]

[†]State Key Laboratory of Rare Earth Resource Utilization, Changchun Institute of Applied Chemistry, Chinese Academy of Sciences, Changchun 130022, People's Republic of China

[‡]University of Chinese Academy of Sciences, Beijing 100049, People's Republic of China

Supporting Information

ABSTRACT: The development of an efficient catalytic electrode toward both hydrogen evolution reaction (HER) and oxygen evolution reaction (OER) is of great significance for overall water splitting associated with the conversion and storage of clean and renewable energy. In this study, carbon paper/carbon tubes/cobalt-sulfide is introduced as an integrated three-dimensional (3D) array electrode for cost-effective and energy-efficient HER and OER in alkaline medium. Impressively, this electrode displays superior performance compared to non-noble metal catalysts reported previously, benefiting from the unique 3D array architecture with increased exposure and accessibility of active sites, improved vectorial electron transport capability, and enhanced release of gaseous products. Such an integrated and versatile electrode makes the overall water splitting proceed in a more direct and smooth manner, reducing the production cost of practical technological devices.

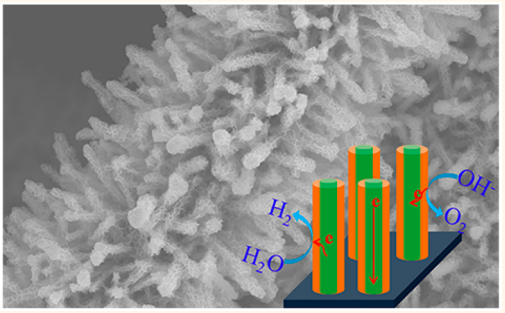

KEYWORDS: *electrocatalysis, integrated 3D electrode, bifunctionality, overall water splitting*

The future of an energy supply based on clean and renewable energy will overcome the reliance on fossil fuels, the current dominating energy source, addressing the challenges of the energy crisis and environment pollution.[1−3] Electricity-driven water splitting into hydrogen and oxygen via water−alkali electrolyzers provides an appealing approach to convert and store abundant but intermittent solar energy, which has drawn intense research interest.[4−6] The widespread implementation hinges on innovative breakthroughs regarding the development of affordable, sustainable, and efficient catalytic materials for two half-reactions, that is, the hydrogen evolution reaction (HER) and the oxygen evolution reaction (OER).[7−9] Currently, state-of-the-art HER and OER catalysts are Pt and RuO_2, respectively, but their long-term availability is questionable owing to the scarcity and subsequent high cost.[10−14] Therefore, substantial efforts have been devoted to develop non-noble transition-metal-based and metal-free electrocatalysts with commensurate performance.[15−21] Heretofore, a series of robust catalysts have been well established for either HER or OER.[22−28] However, in view of the convenience and cost reduction in the overall water splitting, the development of a versatile catalyst enabling the operation in the same electrolyte with satisfying activity toward both HER and OER is technologically important and urgently needed. Recently, the research based on such a thought is proposed but still in its infancy stage.[29−33]

In addition, the conventional preparation of the catalytic electrode requires time- and cost-consuming processes based on planar conductive substrates with a polymer binder to immobilize the active materials, which inevitably results in buried active sites and insufficient mass and electron transport ability, thus impairing the electrocatalytic activity of water splitting. Alternatively, the strategy for directly integrating active materials with current collectors is widely adopted to make an integrated electrode.[34−39] Specifically, well-aligned nanowire (NW) array structures grown on current collectors are extremely interesting owing to their intrinsic advantages, including high exposed surface area, enhanced electron transport, and improved mechanical stability. Indeed, recent research, such as that on $Zn_xCo_{3-x}O_4$ and $Ni_xCo_{3-x}O_4$ NW arrays for OER[40,41] and CoP and CoS_2 NW arrays for HER,[42,43] has been reported. However, considering the semiconducting nature, the vectorial electron transport property of these NWs with length scales even up to

Received: November 11, 2015
Accepted: January 19, 2016
Published: January 19, 2016

DOI: 10.1021/acsnano.5b07126
ACS Nano 2016, 10, 2342−2348

micrometers cannot be guaranteed.[44] Reasonably, the configuration with a built-in electron conductor for the high aspect ratio structure should be seriously considered, maximizing the utilization rate of active materials and further facilitating the reaction kinetics of catalytic electrodes.

With these purposes in mind, herein, an integrated three-dimensional (3D) electrode of carbon paper/carbon tubes/cobalt-sulfide sheets (denoted as CP/CTs/Co-S) has been designed and fabricated, which exhibits high activity and stability toward both HER and OER in alkaline medium, thus behaving as a versatile electrode for efficient overall water splitting.

RESULTS AND DISCUSSION

The 3D conductive substrate of CP/CTs is facilely fabricated *via* a template-assisted method as shown in Scheme 1. Initially,

Scheme 1. Schematic illustration of the fabrication procedure of CP/CTs and corresponding sample photos.

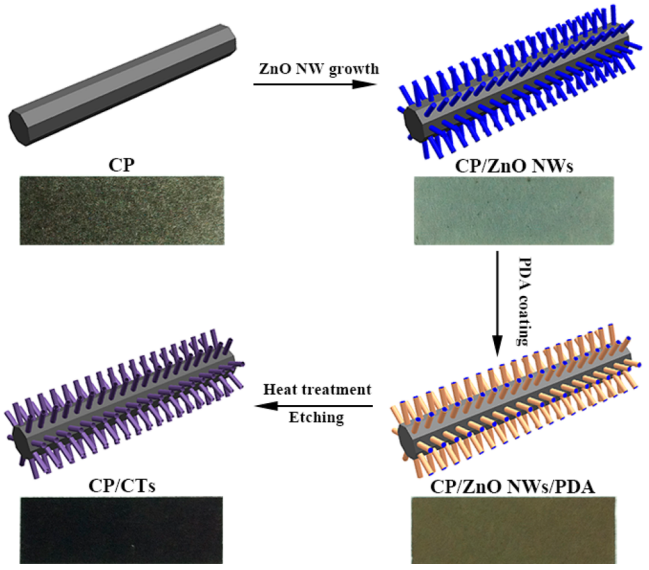

well-aligned ZnO NWs were successfully grown on commercial CP using a wet chemical method, which was verified by the scanning electron microscopy (SEM) images. As shown in Figure 1a and b, CP as a commonly used conductive support has a relatively smooth skeleton, on which the densely packed ZnO NWs are uniformly distributed. These NWs possess a high aspect ratio with diameters of around 200−300 nm and lengths of about 7−10 μm. Subsequently, polydopamine (PDA) is selected as the carbon precursor to coat on the surfaces of the NWs, because it can deposit on virtually any surface through the self-polymerization of dopamine in an alkaline environment.[45,46] Figure 1c reveals that the surface roughness of the NWs is increased after the PDA coating. The typical transmission electron microscopy (TEM) image of an individual NW clearly shows that a thin layer (~28 nm) of PDA evenly covers the surface of ZnO NWs (Figure 1d). Finally, the obtained CP/ZnO NWs/PDA proceeds with the carbonization treatment and acid-washing to generate the targeted 3D conductive CP/CTs substrate. Notably, the CTs well replicate the array structure of ZnO NWs and have direct contact with CP (Figure S1). The derived tube architecture is obviously observed from the characterizations of SEM and TEM (Figure 1e and f). In comparison to the PDA coating, the

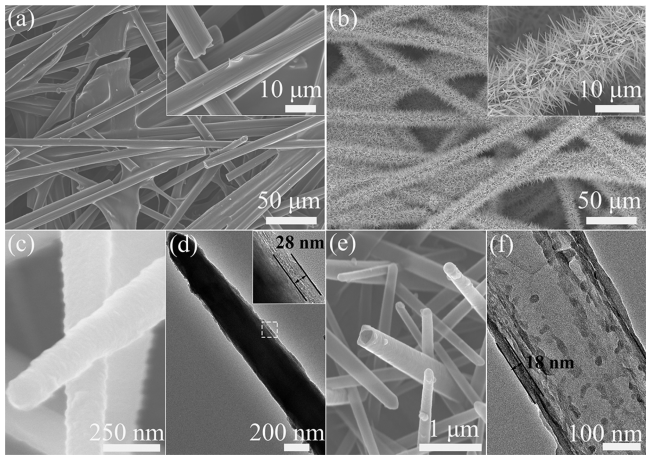

Figure 1. SEM images of (a) CP and (b) CP/ZnO NWs. (c) SEM and (d) TEM images of ZnO NWs/PDA. (e) SEM and (f) TEM images of CTs.

tube wall has a shrinking thickness, which is measured to be ~18 nm. Such a 3D carbonaceous substrate with integrated advantages of high conductivity, high surface area, light weight, and robust physical/chemical stability will be a suitable choice of support electrode for electrochemical reactions.

Cobalt sulfide (Co-S) is selected as the model catalyst because of its promising use as an earth-abundant and inexpensive material for energy conversion and storage.[47−49] Through a facile and scalable chronoamperometric electrodeposition method, the Co-S sheets on a CP/CTs substrate are prepared from the precursor solution containing cobalt nitrate and thiourea at room temperature. After rinsing thoroughly with water/ethanol and annealing under an inert atmosphere, the CP/CTs/Co-S electrode is successfully achieved. Figure 2a shows a typical SEM image of CP/CTs/Co-S, indicating the well-preserved array structure and homogeneous Co-S sheets wrapping the entire CT surface. The thickness of the deposited Co-S layer is ~130 nm, which is coincidentally measured from the cross sectional view of a broken CT/Co-S (Figure 2b). Due to the open spaces of the array structure, Co-S sheets are also partly deposited on the skeleton of CP (Figure S2). The TEM images of a single CT/Co-S also confirm the conformal structure and the thickness (~3 nm) of the Co-S sheet (Figure 2c and d). X-ray diffraction (XRD) is performed to disclose the crystal structure of CP/CTs/Co-S (Figure S3). The XRD pattern of CP/CTs/Co-S shows only the diffraction belonging to carbon, indicating the amorphous nature of Co-S sheets, which is evidenced by the according selected area electron diffraction (SAED) as well (Figure 2e). Thus, more catalytic centers are expected to be created from the coordinatively unsaturated sites of the amorphous Co-S sheets. The energy dispersive X-ray spectroscopy (EDX) indentifies the presence of elements including C, N, O, Co, and S (Figure S4), which are uniformly distributed through a single CT/Co-S, as observed from the element mapping images (Figure 2f). The estimations of the Co content (~1.14 μmol cm^{-2}) and the Co/S ratio (~1.33) are realized by inductively coupled plasma atomic emission spectroscopy (ICP-AES), suggesting probable $CoO/Co(OH)_2$ composites besides CoS_x, which is consistent with the previous reports.[47] This suggestion is verified by X-ray photoelectron spectroscopy (Figure S5). Moreover, the mass loading of Co-S sheets is ~0.32 mg cm^{-2}, determined by the mass difference before and after the electrodeposition using a

DOI: 10.1021/acsnano.5b07126
ACS Nano 2016, 10, 2342−2348

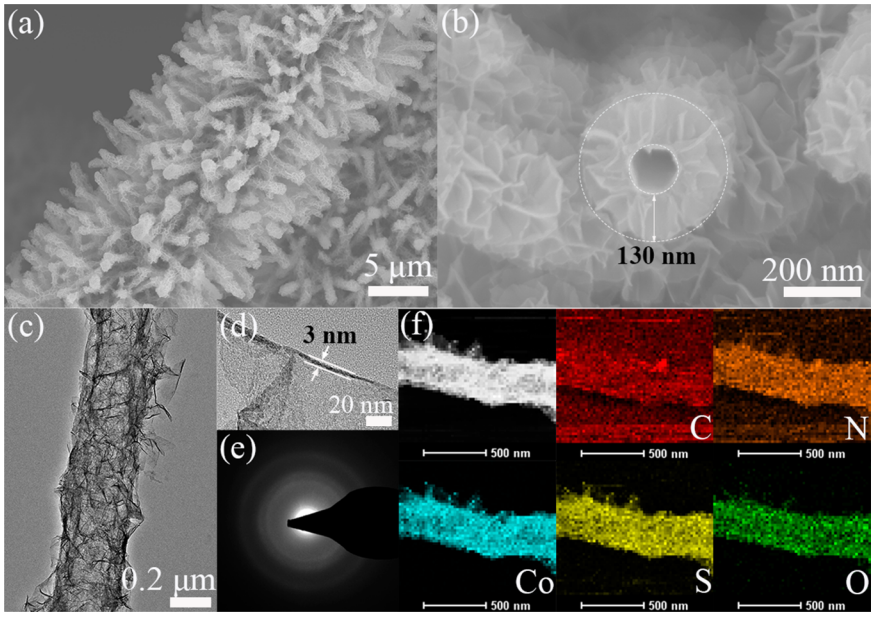

Figure 2. (a, b) SEM images of CP/CTs/Co-S. (c, d) TEM images, (e) SAED pattern, and (f) element mapping of CT/Co-S.

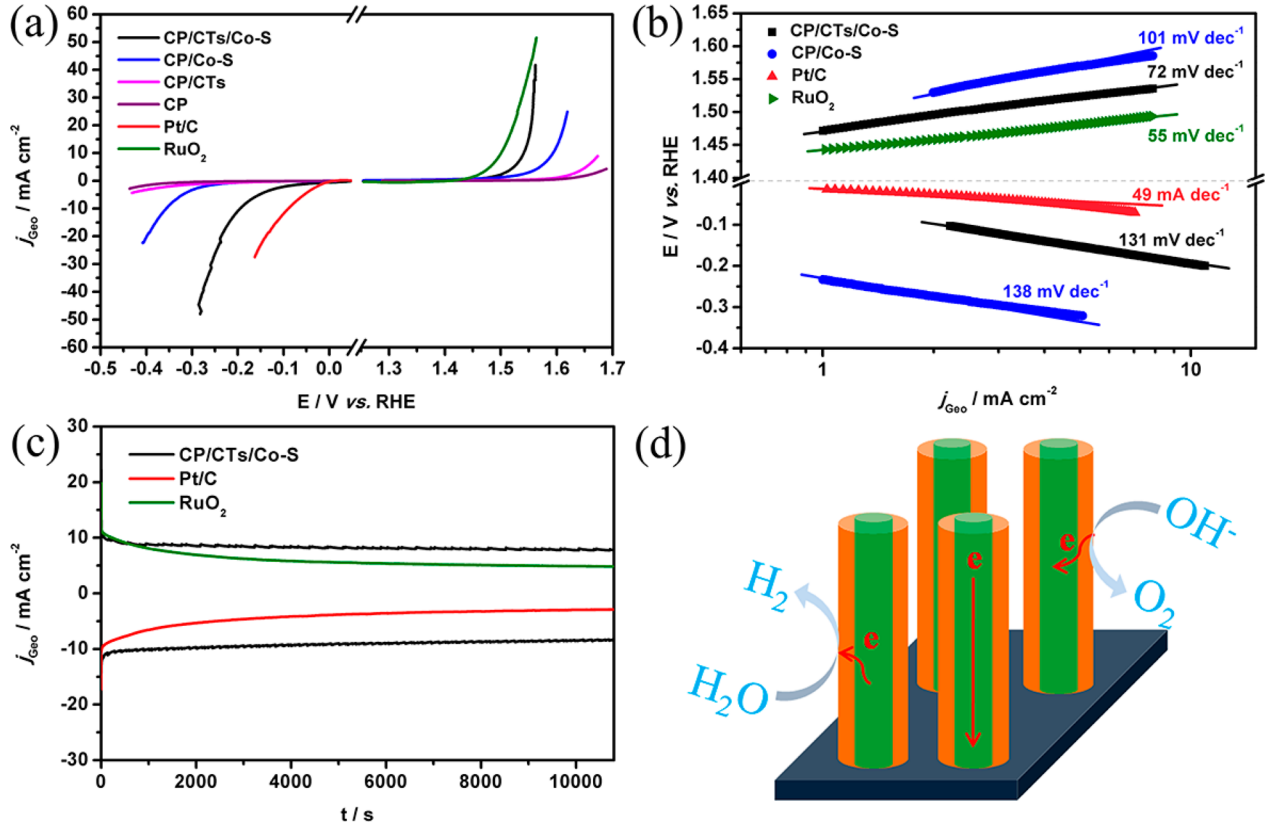

Figure 3. (a) Polarization curves of different catalytic electrodes for HER and OER in 1 M KOH with a scan rate of 2 mV s^{-1}. (b) Corresponding Tafel plots. (c) Chronoamperometric responses of CP/CTs/Co-S, Pt/C, and RuO_2 electrodes at constant potentials for HER and/or OER. (d) Schematic illustration of the operating principle of CP/CTs/Co-S.

microbalance. For comparison, the CP/Co-S electrode with the same mass loading of the Co-S sheets is also prepared *via* electrodeposition. As shown in Figure S6, the dense Co-S sheet film on the CP skeleton has a greater thickness and many cracks, which may result in high contact resistance, limited accessible surface area, and weak stability, implying the deteriorated electrocatalytic performance for water splitting.

The HER and OER activities of as-prepared electrodes are evaluated in 1 M KOH electrolyte using a three-electrode electrochemical configuration with a saturated calomel electrode as the reference electrode and a graphite plate as the counter electrode. All potentials are *iR*-corrected and converted to a reversible hydrogen electrode (RHE) scale *via* calibration (Figure S7). As references, commercial Pt/C (20 wt

DOI: 10.1021/acsnano.5b07126
ACS Nano 2016, 10, 2342−2348

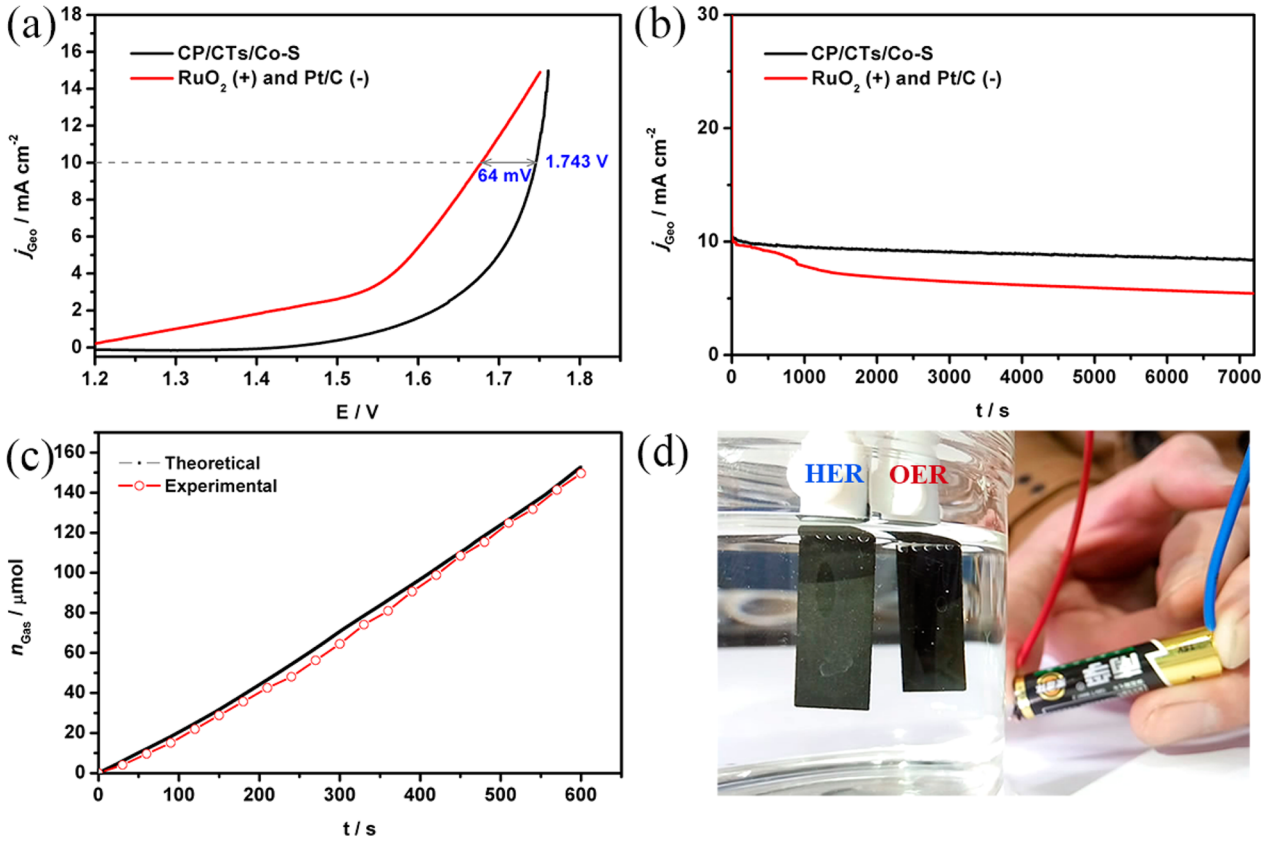

Figure 4. (a) Polarization curves for overall water splitting with a CP/CTs/Co-S electrode as both anode and cathode in 1 M KOH with a scan rate of 2 mV s^{-1}. The benchmarking RuO_2 (+) and Pt/C (−) electrodes are tested side by side. (b) Corresponding chronoamperometric responses of CP/CTs/Co-S electrodes and the benchmarking combination at constant potentials of 1.743 and 1.679 V, respectively. (c) Amount of gaseous products theoretically calculated and experimentally measured *versus* time at the constant potential of 2 V. (d) Optical photograph of overall water splitting powered by an AAA battery with a nominal voltage of 1.5 V.

%) and RuO_2 with the same mass loading on CP are also tested for HER and OER, respectively. As expected, they show superior electrocatalytic activities with negligible overpotentials (Figure 3a). To achieve a current density of 10 mA cm^{-2}, a metric relevant to solar fuel synthesis, CP/CTs/Co-S requires a much lower potential (0.190 V) than CP/Co-S (0.357 V) in the HER process. Also, in the OER process, the potential afforded by CP/CTs/Co-S (1.536 V) to deliver the same current density is more negative than that of CP/Co-S (1.593). Of note, the substrates of CP/CTs and CP contribute little to these activities, confirming that the coating layer of Co-S sheets is dominantly responsible for the high HER and OER activity.

The kinetic activities of the above electrodes are estimated by corresponding Tafel plots (Figure 3b). The Tafel slopes of CP/CTs/Co-S for both HER (131 mV dec^{-1}) and OER (72 mV dec^{-1}) are smaller than those of CP/Co-S, indicating the comparatively favorable catalytic kinetics. Furthermore, the exchange current densities (j_0) are calculated from Tafel plots by an extrapolation method (Figure S8). The j_0 of CP/CTs/Co-S for HER is 3.9×10^{-1} mA cm^{-2}, which is about 16 times that of CP/Co-S (2.4×10^{-2} mA cm^{-2}), and the OER j_0 of CP/CTs/Co-S (8.3×10^{-4} mA cm^{-2}) is greater than that of CP/Co-S (5.8×10^{-4} mA cm^{-2}) as well. Conclusively, CP/CTs/Co-S displays much higher activities than CP/Co-S, benefiting from the 3D array structure. The detailed comparison of the catalytic parameters for these electrodes is shown in Table S1. Although the HER and OER performances of CP/CTs/Co-S are still inferior to those of Pt/C and RuO_2, these are satisfactory for a versatile catalytic electrode and are also competitive with those of non-noble metal-based catalysts reported previously for HER or OER (Tables S2 and S3).

The superior performance of CP/CTs/Co-S, in comparison to that of CP/Co-S, mainly originates from several advantageous aspects, which are the consensuses for the advanced 3D array electrode. First, the internal gaps within the NW arrays increase the accessible surface area, maximizing the exposure of more active sites and enabling a high utilization ratio of catalysts.[40−42,50] The effective surface area can be alternatively reflected by the electrochemical double-layer capacitance (C_{dl}) at the solid−liquid interface. As shown in Figure S9, the C_{dl} of CP/CTs/Co-S is measured to be 103.7 mF cm^{-2}, which is much higher than that of CP/Co-S (29.8 mF cm^{-2}), confirming the larger active surface area of CP/CTs/Co-S. Second, CTs connected to CP provide the built-in continuous pathway for electron transport, decreasing the electron transport distance and barrier and thus facilitating the reaction kinetics.[44] This viewpoint is verified by the electrochemical impedance spectroscopy (Figure S10). The obtained results can be simply fitted with an equivalent circuit consisting of a resistor (R_s) in series with a parallel combination of a resistor (R_{ct}) and a constant phase element, in which R_s and R_{ct} represent the contact resistance and the charge transfer resistance, respectively. Taking the HER process for example, as compared with CP/Co-S, CP/CTs/Co-S displays the lower R_s and R_{ct}, indicative of its favorable electron and charge transport capability. Third, the 3D array configuration promotes the

DOI: 10.1021/acsnano.5b07126
ACS Nano 2016, 10, 2342−2348

release of gas bubbles, enhancing the contact between electrolyte and active sites, which has been experimentally confirmed by previous reports.[39,43] Figure 3d provides a schematic illustration of the above-mentioned advantages for CP/CTs/Co-S.

The turnover frequency (TOF) is a critical indicator of the intrinsic activity for a catalyst. Thus, CP/CTs/Co-S exhibits TOF values of 1.2×10^{-1} s^{-1} at a HER overpotential of 250 mV and 1.6×10^{-2} s^{-1} at an OER overpotential of 300 mV, assuming all the Co sites contribute to the activities. Considering the fact that only accessible sites are active for the reactions, these values are underestimated but still outperform those of many other non-noble metal-based catalysts reported so far (Tables S2 and S3). In addition, the loading amount of the Co-S sheet layer on CP/CTs can be tailored *via* varying the deposition time. The activity measurements reveal that the optimized deposition time is 8 min (Figure S11). Especially, the extension of the deposition time (15 min) results in inferior activity because of the overload of the Co-S sheet layer (Figure S12), highlighting the aforementioned advantages of the 3D array structure again. In view of the practical use, the durability of CP/CTs/Co-S for continuous HER and OER is critically important. To this end, the constant operating potentials initially required to drive the current density of 10 mA cm^{-2} are applied to chronoamperometric tests. Figure 3c reveals that CP/CTs/Co-S displays better HER and/or OER stability than Pt/C and RuO_2, keeping the current densities for over 10 000 s. Moreover, CP/CTs/Co-S also exhibits a fairly stable performance after 1000 continuous potential cycles at an accelerated scan rate of 50 mV s^{-1} (Figure S13). The slight degradation can be mainly attributed to partial S loss and increased $Co(OH)_2$ content (Figures S14 and S15). Even with that, the HER and OER activities of CP/CTs/Co-S after the stability test are superior to those of CP/CTs/$Co(OH)_2$, indicating the Co-S composites are beneficial for water splitting (Figure S16).

Encouraged by the bifunctionality of CP/CTs/Co-S, the overall water splitting is further performed in 1 M KOH using a two-electrode configuration, which is much closer to the practical device. As shown in Figure 4a, CP/CTs/Co-S electrodes afford a current density of 10 mA cm^{-2} at the operating potential of 1.743 V, which is only 64 mV larger than the benchmarking RuO_2 (+) and Pt/C (−) electrodes and comparable to the catalytic materials reported recently for overall water splitting (Table S4). Meanwhile, CP/CTs/Co-S electrodes can withstand continuous electrolysis for at least 7000 s with less degradation than the benchmarking combination (Figure 4b). Additionally, CP/CTs/Co-S electrodes show Faradaic efficiency close to 100% for overall water splitting (Figure 4c). The gaseous products are totally composed of H_2 and O_2, as evidenced by the mass spectrum (Figure S17). Moreover, an AAA battery with a nominal voltage of 1.5 V can drive overall water splitting with obvious gas bubble release, confirming the high efficiency of the CP/CTs/Co-S electrode (Figure 4d and Supplementary Video 1). These results suggest that the CP/CTs/Co-S electrode has potential applications in low-cost and energy-efficient water electrolysis.

CONCLUSIONS

In summary, an integrated CP/CTs/Co-S electrode in a 3D array structure is developed as a cost-effective catalytic electrode, showing remarkable versatility for HER and OER with high activity and stability, which originates from increased exposure and accessibility of active sites, improved vectorial electron transport capability, and enhanced release of gaseous products. Such an integrated and versatile electrode makes the overall water splitting proceed in a more direct and smooth manner, reducing the production cost of the practical technological devices. Our findings will inspire further efforts to develop 3D array structured electrodes with multifunctionality for not only overall water splitting but also other key energy conversion and storage technologies.

EXPERIMENTAL SECTION

Synthesis of CP/ZnO NWs. Briefly, CP was first heat-treated at 500 °C for 1 h in air to increase its wettability. Then, ZnO NWs were grown on CP (6 × 3 cm^2) by a wet chemical process. CP was soaked in an aqueous solution (150 mL) containing 0.1 M $KMnO_4$ for 1 h to form a seed layer. The seeded CP was then dipped into a glass bottle with a precursor solution (100 mL) containing zinc nitrate hexahydrate (15 mM), hexamethylenetetramine (15 mM), and ammonia (4 mL). The sealed bottle was placed into an oven at 90 °C for 24 h. After that, the white-colored CP/ZnO NWs substrate was obtained by water washing and drying at 80 °C for 3 h.

Synthesis of CP/ZnO NWs/PDA. Dopamine hydrochloride (60 mg) was first dissolved in a mixed solution of ethanol (18 mL) and water (20 mL). Then, the as-prepared CP/ZnO NWs substrate was immersed in the mixed solution, to which an ethanol solution (2 mL) containing Tris (60 mg) was added. After 24 h, the brown-colored CP/ZnO NWs/PDA was taken out, rinsed with water and ethanol, and dried at 60 °C for 8 h.

Synthesis of CP/CTs. The CP/ZnO NWs/PDA was calcinated at 800 °C for 1 h under an Ar/H_2 atmosphere. After cooling to room temperature, the substrate was immersed in acid to remove Zn species, followed by water washing and drying at 80 °C for 8 h to obtain CP/CTs.

Preparation of CP/CTs/Co-S. The preparation of CP/CTs/Co-S was achieved *via* the chronoamperometric method using a three-electrode configuration with CP/CTs (1 × 3 cm^2), CP, and Ag/AgCl as working electrode, counter electrode, and reference electrode, respectively. The electrodeposition bath was an ethanol−water solution with a volume ratio of 3:7, containing 0.1 M cobalt nitrate hexahydrate and 0.5 M thiourea. The constant potential of −0.9 V *vs* Ag/AgCl was applied to the CP/CTs electrode (active area: 1 × 2 cm^2) for 8 min. After that, CP/CTs/Co-S was washed with water and ethanol, followed by drying at 60 °C for 8 h and annealing at 300 °C for 1 h under an Ar atmosphere. The mass loading (~0.32 mg cm^{-2}) of Co-S sheets is determined by the mass difference before and after the electrodeposition using a microbalance. Different amounts of the Co-S sheets on the CP/CTs can be tailored by varying the deposition time.

As a control sample, CP/Co-S was also prepared *via* a similar electrodeposition method. The passed charges were controlled and equivalent to that of CP/CTs/Co-S so as to achieve the same mass loading of Co-S sheets.

A 10 mg amount of commercial Pt/C (20 wt %) or RuO_2 was dispersed in diluted Nafion alcohol solution containing 4 mL of ethanol and 50 μL of Nafion, which was then ultrasonicated for 1 h to obtain a homogeneous suspension. Then, the suspension was drop-casted onto CP (1 × 2 cm^2), making the mass loading equivalent to that of the Co-S sheets. Thus, after drying at room temperature, the CP/Pt/C electrode and CP/RuO_2 electrode were applied for HER and OER, respectively.

Characterization. Scanning electron microscopy was performed on a field emission Hitachi S-4800 instrument, operating at an accelerating voltage of 10 kV. Transmission electron microscopy was performed using a FEI Tecnai G2 S-Twin instrument with a field emission gun operating at 200 kV. Powder X-ray diffraction measurement was performed on a Bruker D8 Focus powder X-ray diffractometer using Cu Kα (λ = 0.154 05 nm) radiation (40 kV, 40 mA). X-ray photoelectron spectroscopy (XPS) measurements were

DOI: 10.1021/acsnano.5b07126
ACS Nano 2016, 10, 2342−2348

performed on an ESCALAB 250 photoelectron spectrometer. ICP-AES measurements were performed on a TJA (Thermo Jarrell Ash) Atomscan Advantage instrument. The electrochemical experiments were carried out with a VMP3 electrochemical workstation (Biologic Inc.). Mass analysis of the generated gases was performed using an Ominstar-Thermostar GSD 320 system (Pfeiffer Vacuum) mass spectrometer, wherein Ar is chosen as carrying gas.

Electrochemical Characterization. Electrochemical measurements for HER and OER were performed at room temperature using a three-electrode configuration with CP/CTs/Co-S, a graphite plate, and a saturated calomel electrode as working electrode, counter electrode, and reference electrode, respectively. The polarization curves were obtained in 1 M KOH with a scan rate of 2 mV s^{-1} at room temperature. All potentials were *iR*-compensated to 85% with the built-in program and converted to an RHE scale *via* calibration. The presented current density was normalized to the geometric surface area.

The performance of the CP/CTs/Co-S electrode toward overall water splitting was evaluated in 1 M KOH using a two-electrode configuration. The polarization curve was recorded at a scan rate of 2 mV s^{-1}.

Calculation. The turnover frequency is defined as the number of H_2 or O_2 molecules evolved per site per second:

$$\mathrm{TOF} = \frac{j}{nFN}$$

where j is the measured current density (mA cm^{-2}), n is the mole number of electrons per mole of H_2 or O_2, F is the Faraday constant (96485 C mol^{-1}), and N is the Co content (mol cm^{-2}).

During the overall water splitting, a constant potential (2 V) was applied to the electrodes and the volume of the evolved gas was recorded synchronously using the gas buret. Thus, the Faradaic efficiency is estimated from the observed gas amount and the theoretical gas amount is calculated by the charge passed through the electrode:

$$\text{Faradaic efficiency} = \frac{V_{\text{experimental}}}{V_{\text{theoretical}}} = \frac{V_{\text{experimental}}}{\frac{3}{4} \times \frac{Q}{F} \times V_{\text{m}}}$$

where Q is the charge passed through the electrodes, F is the Faraday constant (96485 C mol^{-1}), the number 4 means 4 moles of electrons per mole of O_2, the number 3 means 3 moles of (H_2 + O_2) per mole of O_2, and V_m is the molar volume of gas (24.5 L mol^{-1}, 298 K, 101 kPa).

ASSOCIATED CONTENT

Supporting Information

The Supporting Information is available free of charge on the ACS Publications website at DOI: 10.1021/acsnano.5b07126.

XRD, EDX, XPS, SEM, mass spectrum, additional electrochemical data, and video of overall water splitting. (PDF)

Movie (WMV)

AUTHOR INFORMATION

Corresponding Author

*E-mail: xbzhang@ciac.ac.cn.

Notes

The authors declare no competing financial interest.

ACKNOWLEDGMENTS

This work is financially supported by the 100 Talents Programme of Chinese Academy of Sciences, National Program on Key Basic Research Project of China (973 Program, Grant Nos. 2012CB215500 and 2014CB932300), and National Natural Science Foundation of China (Grant Nos. 21422108, 21471146, and 21203176).

REFERENCES

(1) Chow, J.; Kopp, R. J.; Portney, P. R. Energy Resources and Global Development. *Science* **2003**, *302*, 1528−1531.

(2) Lewis, N. S.; Nocera, D. G. Powering the Planet: Chemical Challenges in Solar Energy Utilization. *Proc. Natl. Acad. Sci. U. S. A.* **2006**, *103*, 15729−15735.

(3) Jiao, Y.; Zheng, Y.; Jaroniec, M.; Qiao, S. Z. Design of Electrocatalysts for Oxygen- and Hydrogen-Involving Energy Conversion Reactions. *Chem. Soc. Rev.* **2015**, *44*, 2060−2086.

(4) Duan, J.; Chen, S.; Jaroniec, M.; Qiao, S. Z. Heteroatom-Doped Graphene-Based Materials for Energy-Relevant Electrocatalytic Processes. *ACS Catal.* **2015**, *5*, 5207−5234.

(5) Duan, J.; Chen, S.; Jaroniec, M.; Qiao, S. Z. Porous C_3N_4 Nanolayers@N-Graphene Films as Catalyst Electrodes for Highly Efficient Hydrogen Evolution. *ACS Nano* **2015**, *9*, 931−940.

(6) Zhao, Y. F.; Yang, Z. Y.; Zhang, Y. X.; Jing, L.; Guo, X.; Ke, Z.; Hu, P.; Wang, G.; Yan, Y. M.; Sun, K. N. Cu_2O Decorated with Cocatalyst MoS_2 for Solar Hydrogen Production with Enhanced Efficiency under Visible Light. *J. Phys. Chem. C* **2014**, *118*, 14238−14245.

(7) Carmo, M.; Fritz, D. L.; Mergel, J.; Stolten, D. A Comprehensive Review on PEM Water Electrolysis. *Int. J. Hydrogen Energy* **2013**, *38*, 4901−4934.

(8) Chen, S.; Qiao, S. Z. Hierarchically Porous Nitrogen-Doped Graphene-$NiCo_2O_4$ Hybrid Paper as an Advanced Electrocatalytic Water-Splitting Material. *ACS Nano* **2013**, *7*, 10190−10196.

(9) Zheng, Y.; Jiao, Y.; Li, L. H.; Xing, T.; Chen, Y.; Jaroniec, M.; Qiao, S. Z. Toward Design of Synergistically Active Carbon-Based Catalysts for Electrocatalytic Hydrogen Evolution. *ACS Nano* **2014**, *8*, 5290−5296.

(10) Kanan, M. W.; Nocera, D. G. *In Situ* Formation of an Oxygen-Evolving Catalyst in Neutral Water Containing Phosphate and Co^{2+}. *Science* **2008**, *321*, 1072−1075.

(11) Suntivich, J.; May, K. J.; Gasteiger, H. A.; Goodenough, J. B.; Shao-Horn, Y. A Perovskite Oxide Optimized for Oxygen Evolution Catalysis from Molecular Orbital Principles. *Science* **2011**, *334*, 1383−1385.

(12) Voiry, D.; Yamaguchi, H.; Li, J.; Silva, R.; Alves, D. C.; Fujita, T.; Chen, M.; Asefa, T.; Shenoy, V. B.; Eda, G.; Chhowalla, M. Enhanced Catalytic Activity in Strained Chemically Exfoliated WS_2 Nanosheets for Hydrogen Evolution. *Nat. Mater.* **2013**, *12*, 850−855.

(13) Zheng, Y.; Jiao, Y.; Jaroniec, M.; Qiao, S. Z. Advancing the Electrochemistry of the Hydrogen-Evolution Reaction through Combining Experiment and Theory. *Angew. Chem., Int. Ed.* **2015**, *54*, 52−65.

(14) Ma, T. Y.; Ran, J.; Dai, S.; Jaroniec, M.; Qiao, S. Z. Phosphorus-Doped Graphitic Carbon Nitrides Grown *In Situ* on Carbon-Fiber Paper: Flexible and Reversible Oxygen Electrodes. *Angew. Chem., Int. Ed.* **2015**, *54*, 4646−4650.

(15) Li, Y.; Wang, H.; Xie, L.; Liang, Y.; Hong, G.; Dai, H. MoS_2 Nanoparticles Grown on Graphene: An Advanced Catalyst for the Hydrogen Evolution Reaction. *J. Am. Chem. Soc.* **2011**, *133*, 7296−7299.

(16) Chen, W. F.; Sasaki, K.; Ma, C.; Frenkel, A. I.; Marinkovic, N.; Muckerman, J. T.; Zhu, Y.; Adzic, R. R. Hydrogen-Evolution Catalysts Based on Non-Noble Metal Nickel-Molybdenum Nitride Nanosheets. *Angew. Chem., Int. Ed.* **2012**, *51*, 6131−6135.

(17) Popczun, E. J.; Read, C. G.; Roske, C. W.; Lewis, N. S.; Schaak, R. E. Highly Active Electrocatalysis of the Hydrogen Evolution Reaction by Cobalt Phosphide Nanoparticles. *Angew. Chem., Int. Ed.* **2014**, *53*, 5427−5430.

(18) Smith, R. D.; Prevot, M. S.; Fagan, R. D.; Zhang, Z.; Sedach, P. A.; Siu, M. K.; Trudel, S.; Berlinguette, C. P. Photochemical Route for Accessing Amorphous Metal Oxide Materials for Water Oxidation Catalysis. *Science* **2013**, *340*, 60−63.

(19) Gong, M.; Li, Y.; Wang, H.; Liang, Y.; Wu, J. Z.; Zhou, J.; Wang, J.; Regier, T.; Wei, F.; Dai, H. An Advanced Ni-Fe Layered Double Hydroxide Electrocatalyst for Water Oxidation. *J. Am. Chem. Soc.* **2013**, *135*, 8452−8455.

DOI: 10.1021/acsnano.5b07126
ACS Nano 2016, 10, 2342−2348

(20) Zheng, Y.; Jiao, Y.; Zhu, Y.; Li, L. H.; Han, Y.; Chen, Y.; Du, A.; Jaroniec, M.; Qiao, S. Z. Hydrogen Evolution by a Metal-Free Electrocatalyst. *Nat. Commun.* **2014**, *5*, 3783.
(21) Zhao, Y.; Nakamura, R.; Kamiya, K.; Nakanishi, S.; Hashimoto, K. Nitrogen-Doped Carbon Nanomaterials as Non-Metal Electrocatalysts for Water Oxidation. *Nat. Commun.* **2013**, *4*, 2390.
(22) Deng, J.; Ren, P.; Deng, D.; Bao, X. Enhanced Electron Penetration through an Ultrathin Graphene Layer for Highly Efficient Catalysis of the Hydrogen Evolution Reaction. *Angew. Chem., Int. Ed.* **2015**, *54*, 2100−2104.
(23) Ito, Y.; Cong, W.; Fujita, T.; Tang, Z.; Chen, M. High Catalytic Activity of Nitrogen and Sulfur Co-Doped Nanoporous Graphene in the Hydrogen Evolution Reaction. *Angew. Chem., Int. Ed.* **2015**, *54*, 2131−2136.
(24) McCrory, C. C.; Jung, S.; Peters, J. C.; Jaramillo, T. F. Benchmarking Heterogeneous Electrocatalysts for the Oxygen Evolution Reaction. *J. Am. Chem. Soc.* **2013**, *135*, 16977−16987.
(25) Zhao, Y.; Zhao, F.; Wang, X.; Xu, C.; Zhang, Z.; Shi, G.; Qu, L. Graphitic Carbon Nitride Nanoribbons: Graphene-Assisted Formation and Synergic Function for Highly Efficient Hydrogen Evolution. *Angew. Chem., Int. Ed.* **2014**, *53*, 13934−13939.
(26) Liu, Y.; Cheng, H.; Lyu, M.; Fan, S.; Liu, Q.; Zhang, W.; Zhi, Y.; Wang, C.; Xiao, C.; Wei, S.; Ye, B.; Xie, Y. Low Overpotential in Vacancy-Rich Ultrathin $CoSe_2$ Nanosheets for Water Oxidation. *J. Am. Chem. Soc.* **2014**, *136*, 15670−15675.
(27) Zhao, Y.; Sun, B.; Huang, X.; Liu, H.; Su, D.; Sun, K.; Wang, G. Porous Graphene Wrapped CoO Nanoparticles for Highly Efficient Oxygen Evolution. *J. Mater. Chem. A* **2015**, *3*, 5402−5408.
(28) Zhao, Y.; Xie, X.; Zhang, J.; Liu, H.; Ahn, H. J.; Sun, K.; Wang, G. MoS_2 Nanosheets Supported on 3D Graphene Aerogel as a Highly Efficient Catalyst for Hydrogen Evolution. *Chem. - Eur. J.* **2015**, *21*, 15908−15913.
(29) Luo, J.; Im, J. H.; Mayer, M. T.; Schreier, M.; Nazeeruddin, M. K.; Park, N. G.; Tilley, S. D.; Fan, H. J.; Grätzel, M. Water Photolysis at 12.3% Efficiency *via* Perovskite Photovoltaics and Earth-Abundant Catalysts. *Science* **2014**, *345*, 1593−1596.
(30) Ren, J.; Antonietti, M.; Fellinger, T. P. Efficient Water Splitting Using a Simple Ni/N/C Paper Electrocatalyst. *Adv. Energy Mater.* **2015**, *5*, 1401660.
(31) Ledendecker, M.; Clavel, G.; Antonietti, M.; Shalom, M. Highly Porous Materials as Tunable Electrocatalysts for the Hydrogen and Oxygen Evolution Reaction. *Adv. Funct. Mater.* **2015**, *25*, 393−399.
(32) Ma, W.; Ma, R.; Wang, C.; Liang, J.; Liu, X.; Zhou, K.; Sasaki, T. A Superlattice of Alternately Stacked Ni-Fe Hydroxide Nanosheets and Graphene for Efficient Splitting of Water. *ACS Nano* **2015**, *9*, 1977−1984.
(33) Jin, H.; Wang, J.; Su, D.; Wei, Z.; Pang, Z.; Wang, Y. *In Situ* Cobalt-Cobalt Oxide/N-Doped Carbon Hybrids as Superior Bifunctional Electrocatalysts for Hydrogen and Oxygen Evolution. *J. Am. Chem. Soc.* **2015**, *137*, 2688−2694.
(34) Kong, D.; Wang, H.; Lu, Z.; Cui, Y. $CoSe_2$ Nanoparticles Grown on Carbon Fiber Paper: An Efficient and Stable Electrocatalyst for Hydrogen Evolution Reaction. *J. Am. Chem. Soc.* **2014**, *136*, 4897−4900.
(35) Peng, S.; Li, L.; Han, X.; Sun, W.; Srinivasan, M.; Mhaisalkar, S. G.; Cheng, F.; Yan, Q.; Chen, J.; Ramakrishna, S. Cobalt Sulfide Nanosheet/Graphene/Carbon Nanotube Nanocomposites as Flexible Electrodes for Hydrogen Evolution. *Angew. Chem., Int. Ed.* **2014**, *53*, 12594−12599.
(36) Wang, J.; Zhong, H. X.; Qin, Y. L.; Zhang, X. B. An Efficient Three-Dimensional Oxygen Evolution Electrode. *Angew. Chem., Int. Ed.* **2013**, *52*, 5248−5253.
(37) Chen, S.; Duan, J.; Jaroniec, M.; Qiao, S. Z. Three-Dimensional N-Doped Graphene Hydrogel/NiCo Double Hydroxide Electrocatalysts for Highly Efficient Oxygen Evolution. *Angew. Chem., Int. Ed.* **2013**, *52*, 13567−13570.
(38) Trotochaud, L.; Ranney, J. K.; Williams, K. N.; Boettcher, S. W. Solution-Cast Metal Oxide Thin Film Electrocatalysts for Oxygen Evolution. *J. Am. Chem. Soc.* **2012**, *134*, 17253−17261.
(39) Lu, Z.; Zhu, W.; Yu, X.; Zhang, H.; Li, Y.; Sun, X.; Wang, X.; Wang, H.; Wang, J.; Luo, J.; Lei, X.; Jiang, L. Ultrahigh Hydrogen Evolution Performance of Under-Water "Superaerophobic" MoS_2 Nanostructured Electrodes. *Adv. Mater.* **2014**, *26*, 2683−2687.
(40) Liu, X.; Chang, Z.; Luo, L.; Xu, T.; Lei, X.; Liu, J.; Sun, X. Hierarchical $Zn_xCo_{3-x}O_4$ Nanoarrays with High Activity for Electrocatalytic Oxygen Evolution. *Chem. Mater.* **2014**, *26*, 1889−1895.
(41) Li, Y.; Hasin, P.; Wu, Y. $Ni_xCo_{3-x}O_4$ Nanowire Arrays for Electrocatalytic Oxygen Evolution. *Adv. Mater.* **2010**, *22*, 1926−1929.
(42) Tian, J.; Liu, Q.; Asiri, A. M.; Sun, X. Self-Supported Nanoporous Cobalt Phosphide Nanowire Arrays: An Efficient 3D Hydrogen-Evolving Cathode over the Wide Range of pH 0−14. *J. Am. Chem. Soc.* **2014**, *136*, 7587−7590.
(43) Faber, M. S.; Dziedzic, R.; Lukowski, M. A.; Kaiser, N. S.; Ding, Q.; Jin, S. High-Performance Electrocatalysis Using Metallic Cobalt Pyrite (CoS_2) Micro- and Nanostructures. *J. Am. Chem. Soc.* **2014**, *136*, 10053−10061.
(44) Chen, Z.; Cummins, D.; Reinecke, B. N.; Clark, E.; Sunkara, M. K.; Jaramillo, T. F. Core-Shell MoO_3-MoS_2 Nanowires for Hydrogen Evolution: A Functional Design for Electrocatalytic Materials. *Nano Lett.* **2011**, *11*, 4168−4175.
(45) Lee, H.; Dellatore, S. M.; Miller, W. M.; Messersmith, P. B. Mussel-Inspired Surface Chemistry for Multifunctional Coatings. *Science* **2007**, *318*, 426−430.
(46) Liu, Y.; Ai, K.; Lu, L. Polydopamine and Its Derivative Materials: Synthesis and Promising Applications in Energy, Environmental, and Biomedical Fields. *Chem. Rev.* **2014**, *114*, 5057−5115.
(47) Sun, Y.; Liu, C.; Grauer, D. C.; Yano, J.; Long, J. R.; Yang, P.; Chang, C. J. Electrodeposited Cobalt-Sulfide Catalyst for Electrochemical and Photoelectrochemical Hydrogen Generation from Water. *J. Am. Chem. Soc.* **2013**, *135*, 17699−17702.
(48) Kornienko, N.; Resasco, J.; Becknell, N.; Jiang, C. M.; Liu, Y. S.; Nie, K.; Sun, X.; Guo, J.; Leone, S. R.; Yang, P. *Operando* Spectroscopic Analysis of an Amorphous Cobalt Sulfide Hydrogen Evolution Electrocatalyst. *J. Am. Chem. Soc.* **2015**, *137*, 7448−7455.
(49) Wang, M.; Anghel, A. M.; Marsan, B.; Cevey Ha, N. L.; Pootrakulchote, N.; Zakeeruddin, S. M.; Grätzel, M. CoS Supersedes Pt as Efficient Electrocatalyst for Triiodide Reduction in Dye-Sensitized Solar Cells. *J. Am. Chem. Soc.* **2009**, *131*, 15976−15977.
(50) Ma, T. Y.; Dai, S.; Jaroniec, M.; Qiao, S. Z. Metal-Organic Framework Derived Hybrid Co_3O_4-Carbon Porous Nanowire Arrays as Reversible Oxygen Evolution Electrodes. *J. Am. Chem. Soc.* **2014**, *136*, 13925−13931.

DOI: 10.1021/acsnano.5b07126
ACS Nano 2016, 10, 2342−2348